


# Dorsal column and root stimulation at A $\beta$ -fiber intensity activate superficial dorsal horn glutamatergic and GABAergic populations

Molecular Pain  
Volume 18: 1–13  
© The Author(s) 2022  
Article reuse guidelines:  
[sagepub.com/journals-permissions](https://sagepub.com/journals-permissions)  
DOI: 10.1177/17448069221079559  
[journals.sagepub.com/home/mpx](https://journals.sagepub.com/home/mpx)  


Wei Fan, Steve J Sullivan, and Andrei D Sdrulla 

## Abstract

Neurostimulation therapies are frequently used in patients with chronic pain conditions. They emerged from Gate Control Theory (GCT), which posits that A $\beta$ -fiber activation recruits superficial dorsal horn (SDH) inhibitory networks to “close the gate” on nociceptive transmission, resulting in pain relief. However, the efficacy of current therapies is limited, and the underlying circuits remain poorly understood. For example, it remains unknown whether ongoing stimulation of A $\beta$ -fibers is sufficient to drive activity in SDH neurons. We used multiphoton microscopy in spinal cords extracted from mice expressing the genetically encoded calcium indicator GCaMP6s in glutamatergic and GABAergic populations; activity levels were inferred from deconvolved calcium signals using CalmAn software. Sustained A $\beta$ -fiber stimulation at the dorsal columns or dorsal roots drove robust yet transient activation of both SDH populations. Following the initial increase, activity levels decreased below baseline in glutamatergic neurons and were depressed after stimulation ceased in both populations. Surprisingly, only about half of GABAergic neurons responded to A $\beta$ -fiber stimulation. This subset showed elevated activity for the entire duration of stimulation, while non-responders decreased with time. Our findings suggest that A $\beta$ -fiber stimulation initially recruits both excitatory and inhibitory populations but has divergent effects on their activity, providing a foundation for understanding the analgesic effects of neurostimulation devices.

Perspective: This article used microscopy to characterize the responses of mouse spinal cord cells to stimulation of non-painful nerve fibers. These findings deepen our understanding of how the spinal cord processes information and provide a foundation for improving pain-relieving therapies.

## Keywords

Multiphoton microscopy, superficial dorsal horn, gate control theory, A $\beta$ -fiber stimulation, spinal cord stimulation

Date Received: 19 August 2021; accepted: 20 January 2022

## Introduction

Spinal cord and peripheral nerve stimulation are neuro-modulation therapies frequently used to treat chronic refractory pain. These approaches emerged from Gate Control Theory (GCT), the most influential theoretical concept in the pain field. GTC states that activation of A $\beta$ -fibers “closes the gate” on pain by enhancing inhibitory drive in the superficial dorsal horn (SDH).<sup>1</sup> Despite the longevity of GCT, no studies directly addressed whether sustained stimulation of A $\beta$ -fibers is sufficient to drive activity in SDH neurons, primarily because of the vulnerability of electrophysiological recordings to the

electrical artifact generated by continuous stimulation.<sup>2,3</sup> Multiple publications have indirectly supported that A $\beta$ -fiber stimulation modulates spinal cord neurons. For example,

---

Department of Anesthesiology and Perioperative Medicine, Oregon Health & Science University, Portland, OR, USA

### Corresponding Author:

Andrei Sdrulla, Department of Anesthesiology and Perioperative Medicine  
Oregon Health & Science University, L459 3181 S.W. Sam Jackson Park  
Road, Portland, OR 97239, USA.  
Email: [sdrulla@ohsu.edu](mailto:sdrulla@ohsu.edu)



Creative Commons Non Commercial CC BY-NC: This article is distributed under the terms of the Creative Commons Attribution-NonCommercial 4.0 License (<https://creativecommons.org/licenses/by-nc/4.0/>) which permits non-commercial use, reproduction and distribution of the work without further permission provided the original work is attributed as specified on the SAGE and Open Access pages (<https://us.sagepub.com/en-us/nam/open-access-at-sage>).

dorsal column stimulation (DCS) increased GABA,<sup>4,5</sup> and depressed excitatory neurotransmitter levels in the spinal cord in rats.<sup>4</sup> A one-second-long train of DCS, at a frequency most commonly employed clinically (50 Hz), was sufficient to activate SDH neurons in cats—although the identity of the recorded cells was not explored.<sup>6</sup> Studies looking at immediate-early gene expression following DCS have been equivocal: some found expression of *c-fos* throughout the spinal cord,<sup>7,8</sup> whereas others only observed increased immunoreactivity in regions distal to the electrode at lower frequencies (4 Hz).<sup>9</sup>

The neurons residing in the SDH can be functionally divided into excitatory and inhibitory populations, based on the expression of VGlut2 (vesicular glutamate transporter) and *Viaat* (vesicular inhibitor amino acid transporter), respectively.<sup>10,11</sup> These populations are critical for developing and maintaining chronic pain states.<sup>12–15</sup> Thus, it remains to be determined whether sustained activation of A $\beta$ -fibers, using clinically relevant stimulation waveforms, is sufficient to modulate activity in GABAergic and glutamatergic SDH populations.

Optical approaches combined with advancements in protein-based indicators such as GCaMP6 have overcome many of the limitations of electrical recordings and revolutionized our understanding of neuronal circuits.<sup>16–20</sup> These techniques have been implemented to image molecularly defined brain and spinal cord populations.<sup>21–23</sup> The application of these tools presents a unique opportunity to dissect the effects of continuous A $\beta$ -fiber stimulation on SDH neurons and provides a cellular basis for how it mediates analgesia.<sup>21</sup>

We constructed a miniaturized bipolar epidural DCS electrode and identified physiological stimulation parameters *in vivo* and *in vitro*. We imaged neuronal activity *ex vivo* in the thoracolumbar spinal cord blocks extracted from mice expressing GCaMP6s in glutamatergic and GABAergic neurons. DCS and dorsal root stimulation (DRS) at A $\beta$ -fiber intensities activated both populations, although only transiently. In glutamatergic neurons, we observed biphasic responses with a robust initial increase followed by decreased activity during and after stimulation. We observed that only about half of the GABAergic neurons responded to stimulation; this subset had sustained activity levels above baseline for the entire duration of stimulation. Our findings support the hypothesis that activation of A $\beta$ -fibers differentially activates SDH networks and, for the first time, provide direct evidence that DCS and DRS can drive sustained activity in GABAergic interneurons.

## Methods

All experiments were approved by the Institutional Animal Care and Use Committee at Oregon Health and Science University.

### Mouse strains

VGlut2-Cre mice (Stock No: 016963, *Vglut2-cre* knock-in; The Jackson Laboratory) were crossed with homozygous

floxed GCaMP6s mice (derived from strain Ai96; Stock No: 024106; The Jackson Laboratory, Bar Harbor, ME), resulting in GCaMP6s expression in glutamatergic neurons. To drive expression of GCaMP6s in GABAergic interneurons, we crossed *Viaat-Cre* mice (Stock No: 016962; The Jackson Laboratory) with homozygous GCaMP6s mice. The mice were kept under standard colony conditions, with 12-h day/night cycles, and had access to food and water *ad libitum*. Both males and females were used.

## Fabrication and validation of a bipolar dorsal column stimulation electrode

### Bipolar electrode construction

The electrode was constructed from two pieces of 36-gauge gold wire (catalog # 751,000, A-M Systems, Sequim, Washington) sandwiched between 0.5 mil (13  $\mu$ m thick) Kapton tape (Caplinq, Ontario, CA). The electrode dimensions were as follows: width 1 mm, length 2.5 mm, and thickness 150  $\mu$ m, cut to size with an 11 blade scalpel under a standard dissection microscope. The exposed gold wire segments measured 0.5 mm and were separated by a distance of 0.5 mm from the caudal end of the superior segment to the rostral end of the inferior one. The electrode template was etched in stainless steel to help standardize electrode construction (custom designed from ponoko.com).

### *In vivo* spinal cord stimulation and sciatic compound action potential recording

Adult *Viaat/GCaMP6s* mice (6–8 weeks old) were used for these experiments. Isoflurane anesthesia was induced (5%) and maintained at 2% for the duration of the experiments. The mice were endotracheally intubated with a 20G angiocath (Braun, Melsungen, Germany) and ventilated for the duration of the experiments (tidal volume 260  $\mu$ L, rate 240 breaths/min; MiniVent Type 845, Hugo Sachs Elektronik, March-Hugstetten, Germany). Body temperature was monitored with a rectal thermometer probe (Model BAT-12, Physitemp, Clifton, NJ) and maintained (35–36°C) with a circulating water heating pad (T/Pump Professional, Stryker, MI). Heart rate was monitored continuously via needle electrodes. The thoracic curvature prominence (~T11, corresponding to the L1/2 segment) was exposed, and the interlaminar space was accessed with blunt and sharp dissection. A custom bipolar electrode (described above) was gently inserted in the epidural space and sutured to the fascia. The skin was closed with interrupted sutures (5–0 Polysorb, Covidien, Dublin, Ireland). Spinal cord stimulation (30 biphasic charge-balanced pulses at 50 Hz with equal negative and positive phases, each 0.2 ms duration) was delivered via the epidural electrode using an isolated stimulator (Model 4100, A-M Systems, Sequim, Washington), allowing us to determine the motor threshold amplitude. The stimulation amplitude was

gradually increased in 10  $\mu$ A steps until a visible twitch or contraction was noted at the trunk or limbs. This value was recorded as the motor threshold. Once the motor threshold was established, the sciatic nerve was exposed at the mid-thigh by carefully separating the gluteus maximus and biceps femoris muscles. A stainless steel hook electrode was carefully placed around the nerve, and a ground needle electrode was placed in the nearby tissue. Warm mineral oil was used to cover the hook electrode. Then, the mouse was paralyzed with pancuronium (1 mg/kg). Five bipolar square pulses (1 Hz) were delivered via the epidural electrode, and the resulting compound action potentials (cAP) were amplified using a CyberAmp320 amplifier, digitized, and recorded using Spike2 software. The stimulation strength was gradually increased until cAPs were clearly observed. cAPs were averaged offline using Matlab (Mathworks, Natick, MA). To standardize our protocol for detection of cAP thresholds, we measured the variance of the signal within a 2 ms window before the stimulation was delivered and compared it with a similar window starting after the stimulation artifact returned to baseline. The stimulation threshold for evoking a sciatic nerve cAP was defined as the amplitude where a significant difference was present in the variance test ( $p < 0.01$ ) between the two regions. Conduction velocities were measured by dividing the estimated distance between stimulation and recording sites by the latency from the start of the stimulation to the first peak of the cAP.

### *In vitro compound action potential recording*

The lumbar spinal cord was extracted as described below from adult (five-to seven-week-old) *Viaat/GCaMP6s* mice, and the DCS electrode was placed over the dorsal columns near the L1/2 segments. Five square pulses (0.2 ms) were delivered at 1 Hz using a stimulus isolator (A365, WPI, Sarasota, FL) driven by pClamp software (Molecular Devices, San Jose, CA). The cAPs were recorded at the dorsal roots via tight-fitting, thin-wall glass pipettes (1.2 mm diameter, Sutter Instruments, Novato, CA) backfilled with ACSF and attached via suction. Signals were amplified and digitized (MultiClamp 700, Molecular Devices, San Jose, CA) and analyzed offline using Matlab (Mathworks, Natick, MA). Conduction velocities were measured by dividing the estimated distance between stimulation and recording sites by the latency from the start of the stimulation to the first peak of the cAP.

### *Lumbar spinal cord preparation for electrophysiology and imaging experiments*

Five-to seven-week-old *Viaat/GCaMP6s* or *VGlut2/GCaMP6s* mice of both sexes were deeply anesthetized with 5% isoflurane and decapitated. The lumbar spinal cord was rapidly removed en bloc and placed in oxygenated ACSF (in mM: 125 NaCl, 2.5 KCl, 26 NaHCO<sub>3</sub>, 1.25 NaH<sub>2</sub>PO<sub>4</sub>H<sub>2</sub>O, 1 MgCl<sub>2</sub>, 2 CaCl<sub>2</sub>, and 25 glucose) at room temperature. The dorsal roots were trimmed, and the dura was removed. The tissue

block was glued to a thick glass rectangle and perfused with room temperature, oxygenated ACSF at 3 mL/min during experiments.

### *Dorsal column and dorsal root stimulation*

Dorsal column stimulation was delivered via our custom-made electrode applied to the dorsal columns at L1/2 *in vitro*, in lumbar spinal cords obtained from mice of both sexes. Stimulation was delivered using a stimulus isolator (A365, WPI, Sarasota, FL) driven by a waveform generator (Pulsemaster A300, WPI). DRS was delivered via a tight-fitting, thin-wall glass pipette (1.2 mm diameter; Sutter Instruments, Novato, CA) backfilled with ACSF and attached to the root via suction, typically at L4. DCS was delivered as charge-balanced square biphasic pulses (equal negative and positive phases, 0.2 ms duration each) at 50 Hz unless otherwise specified. DRS consisted of square pulses (0.2 ms duration) at 50 Hz.

### *Multiphoton microscopy and image analysis*

The imaging system consisted of a Zeiss 7 MP microscope (Zeiss Instruments, Thornwood, NY) equipped with a femtosecond-pulsed tunable Ti:Sapphire laser (Coherent, Santa Clara, CA), tuned to a wavelength of 940 nm (<40 mW at back aperture), and a 512  $\times$  512 field of view. Fluorescence images were acquired using a 20X/1.0 water immersion objective at  $\sim$ 3 Hz. Neurons residing in a volume 50–100  $\mu$ m deep from the surface of the dorsal horn at L3 were imaged for both DCS or DRS unless otherwise specified. The optical plane with the most neurons responding to a test stimulation was selected, with at least 10 min between imaging sessions. Tissue drift was generally minimal. The image analysis software CalmAn was used for image processing, including motion correction, neuron outline, and deconvolution of the spike rates.<sup>24,25</sup> Standard settings were used for the constrained non-negative matrix factorization method, and we observed robust results that were comparable with manual neuronal outline and signal extraction.<sup>21</sup> Inferred spike rates obtained from CalmAn were analyzed using custom Matlab functions and plotted using Prism (GraphPad, San Diego, CA). The spike rates have arbitrary units and do not represent actual spike counts; instead, they are a measure of deconvolved neural activity that is proportional to the firing rates of the neurons at each time.<sup>26</sup> Responder neurons were defined as having a 50% increase in spike rates during a window 10 s after the stimulation started. To bin neuronal activity, responses were averaged every 1 min.

### **Statistics**

Data are shown as mean  $\pm$  SEM unless otherwise indicated. Data analysis was performed in Prism. Activity levels were compared to pre-stimulation levels using repeated measures ANOVA (RM ANOVA) followed by Dunnett's multiple comparisons test. Between-group experiments were compared using two-way ANOVA followed by Sidak's multiple

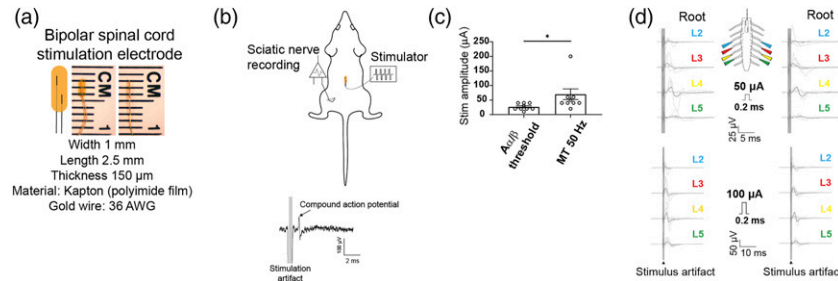


**Figure 1.** Dorsal column stimulation activates A $\beta$ -fibers *in vivo* and *in vitro*. (a) A mouse-sized bipolar electrode was created from gold wires and thin Kapton tape with the dimensions listed. (b) The bipolar electrode was placed in the epidural space in anesthetized *Viaat/GCaMP6s* mice. The motor threshold to 50 Hz stimulation was determined using charge-balanced biphasic pulses and increasing amplitudes. Retrogradely transmitted compound action potentials were recorded at the sciatic nerve. (c) The amplitude required to elicit motor responses (motor threshold) was significantly higher than that required to evoke a compound action potential ( $n = 9$ ; Student's *t*-test,  $p < 0.05$ ). (d) Dorsal column stimulation evoked retrogradely transmitted action potentials at the dorsal roots. The custom-made electrode described in a) was placed on the dorsal columns in spinal cord blocks from *Viaat/GCaMP6s* mice. Brief square pulses (0.2 ms duration) were delivered at amplitudes of 50 (upper panel) and 100  $\mu\text{A}$  (lower panel). The compound action potentials were measured at the dorsal roots shown in the diagram on the corresponding side. The dark line represents the average trace.  $N = 6$ .

comparisons test. For *in vivo* experiments, the motor thresholds were compared using unpaired two-tailed *t*-tests. The fractions of responder neurons were compared using Chi-squared tests.

## Results

### Generation and testing of a miniaturized bipolar epidural stimulation electrode *in vivo* and *in vitro*

We developed and validated an epidural DCS electrode appropriately sized for mice. As the dimensions of the electrode were a major limiting factor, we used Kapton (polyimide tape) and thin gold wire to achieve a thickness of 150  $\mu\text{m}$  (Figure 1). The electrodes were implanted without difficulty in anesthetized mice and used to deliver charge-balanced square biphasic pulses at 50 Hz. We used this frequency as it is the most commonly used in clinical practice<sup>27,28</sup> and in mechanistic animal studies.<sup>21,29–32</sup> Motor thresholds were measured by gradually increasing the DCS amplitude until a response was observed. We then measured compound action potentials at the sciatic nerve using the same range of stimulation parameters. Action potentials with fast conduction velocities (CV) were clearly distinguished (CV  $22.30 \pm 2.92$  m/s,  $n = 10$ ), supporting the activation of A $\beta$ -fibers and retrograde propagation (Figure 1(b)). The threshold for evoking action potentials was  $26.67 \pm 11.18$   $\mu\text{A}$ , which was significantly less than the motor threshold ( $71.11 \pm 20.37$   $\mu\text{A}$ ,  $n = 9$ ;  $p < 0.05$ ). Thus, our bipolar electrode activated A $\beta$ -fibers and elicited motor responses, supporting its usefulness for exploring DCS biology.

Next, we established the ability of our electrode to activate dorsal column fibers *in vitro* (Figure 1(d)). This is important, as current shunting may occur through the ACSF bathing the spinal cord, with diminished flow through tissue and decreased activation of adjacent dorsal column axons. The electrode was positioned over the dorsal columns spanning the L1/2 segments, and brief square pulses were delivered at amplitudes of 50 and

100  $\mu\text{A}$ . These amplitudes were selected to approximate the A $\beta$ -fiber and motor thresholds measured *in vivo*, respectively. We observed retrogradely transmitted action potentials on both sides of the spinal cord at all the dorsal roots examined (L2–L5). The conduction velocities at left and right L5 dorsal roots were compared for the 100  $\mu\text{A}$  stimulation amplitude, and no differences were found (CV left L5 =  $13.52 \pm 2.03$  m/s, right L5 =  $15.18 \pm 2.38$  m/s;  $p > 0.05$ ;  $n = 6$  mice). These findings validated the use of our bipolar electrode to activate dorsal column fibers *in vitro*.

### Tonic dorsal column stimulation transiently activates glutamatergic and GABAergic populations

We imaged SDH neurons in lumbar spinal cord segments from mice expressing *GCaMP6s* in either glutamatergic or GABAergic neurons and inferred activity (deconvolved spikes rates) from calcium fluorescence with the software *CaImAn* (Figures 2(a)–(c)).<sup>24</sup> Spontaneous activity levels were stable over the duration of the imaging period in both populations (Figure 2(d)).

We delivered DCS at 50 Hz continuously for 3 min. This stimulation duration was selected as it allows stable imaging of the same neurons (due to negligible drift) and minimizes photobleaching. We observed a pronounced activation of glutamatergic neurons when using a stimulation amplitude of 100  $\mu\text{A}$  (Figure 2(c) and Figure 3). We also observed responses at an amplitude of 50  $\mu\text{A}$ , but they were less prominent (data not shown). As demonstrated in Figure 3(Ab), DCS produced a profound but transient activation that lasted seconds. We binned spike rates every minute and observed an initial increase, followed by a decrease to below pre-stimulation levels (inferred spike rate:  $7.17 \pm 0.38$  at minute 1 vs  $12.94 \pm 0.42$  at minute 2,  $5.43 \pm 0.34$  at minute 3,  $5.17 \pm 0.34$  at minute 4;  $p < 0.0001$ ;  $n = 258$  neurons from five mice; Figure 3(Ac)). Firing rates further decreased after the stimulation ended ( $3.02 \pm 0.34$  at 5 min,

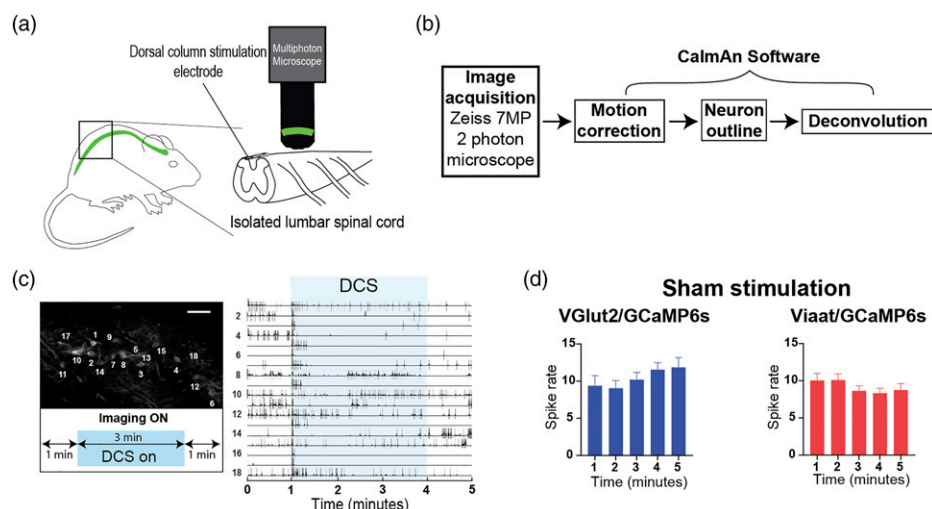


**Figure 2.** Imaging glutamatergic and GABAergic activity in the superficial dorsal horn. (a) The spinal cord was dissected from transgenic mice expressing GCaMP6s and imaged *in vitro*. The custom-made electrode was applied to the dorsal columns. Dorsal column stimulation (DCS; 100  $\mu$ A, 50 Hz, 0.2 ms charge-balanced biphasic pulses) was delivered at L1/2, and superficial dorsal horn neuronal activity was imaged distally at L3. (b) Image acquisition, processing, and analysis pipeline. A Zeiss multiphoton microscope was used to acquire the images. Post-processing and spike rate deconvolution was accomplished with the image analysis software CalmAn. (c) Example glutamatergic responses to dorsal column stimulation delivered for 3 min. The left panel is a max projected image of the 5-min long time series. The right panel shows the raw fluorescence traces (darker lines) overlaid on inferred spiking (traces individually scaled; numbers corresponding to the neurons in the image). Scale bar 50  $\mu$ m. (d) The activity of glutamatergic and GABAergic neurons residing in the superficial dorsal horn was measured continuously for 5 min in the absence of stimulation. There was no significant change in activity over time for either population via RM ANOVA (VGlut2/GCaMP6s group: F (4, 56) = 1.65,  $p$  = 0.20;  $n$  = 61 neurons from 4 mice. Viat/GCaMP6s group: F (4, 124) = 1.93,  $p$  = 0.15;  $n$  = 129 neurons from five mice).

$p < 0.0001$ ). Thus, DCS transiently activated and then depressed SDH glutamatergic neurons.

Next, we imaged the activity of GABAergic SDH neurons. As with glutamatergic neurons, we observed a significant increase in activity (Figure 3(Ba–b)) that concurred with the start of stimulation. The elevated neuronal firing was transient and then returned to baseline for the rest of the stimulation period. As with glutamatergic cells, spike rates decreased below baseline once the stimulation was turned off (10.82  $\pm$  0.62 at 1 min versus 8.02  $\pm$  0.54 at 5 min,  $p < 0.01$ ;  $n$  = 327 neurons from six mice). The short-lived activation of GABAergic neurons was surprising as DCS is thought to drive sustained firing in inhibitory neurons, as hypothesized in GCT. In sum, DCS generated robust but transient activation of both glutamatergic and GABAergic SDH networks.

### Dorsal root stimulation at A $\beta$ -fiber intensity transiently activates glutamatergic and GABAergic populations

We pursued experiments where A $\beta$ -fiber stimulation was delivered at the dorsal root to ask whether activation of A $\beta$ -fibers peripherally had similar effects to central stimulation (DCS) and in order to avoid direct recruitment of neuropil adjacent to the dorsal column electrode.<sup>2</sup> We used a pipette tightly attached to the L4 dorsal root and a stimulation intensity (20  $\mu$ A, 0.2 ms) previously shown to activate large myelinated axons preferentially.<sup>30</sup> SDH neurons residing at the L3 segment were imaged (Figure 4). As with DCS, DRS

elicited an intense but brief activation of glutamatergic neurons (Figure 4(c)). During the first minute, glutamatergic activity increased significantly (inferred spike rate: 7.11  $\pm$  0.29 at baseline vs 12.70  $\pm$  0.41 at minute 2,  $p < 0.0001$ ;  $n$  = 475 from six mice). Activity decreased from pre-stimulation levels during the second minute of DRS (6.26  $\pm$  0.26) and was further attenuated once stimulation was turned off (3.92  $\pm$  0.23 at minute 5). Overall, DRS and DCS resulted in similar patterns of activation and inhibition of glutamatergic SDH neurons.

Similar experiments were conducted in labeled GABAergic neurons (Figure 4(d)). DRS resulted in a transient increase in activity during the first minute of stimulation (7.06  $\pm$  0.49 at baseline vs 11.89  $\pm$  0.57 at minute 1,  $p < 0.0001$ ;  $n$  = 184 from six mice). Activity levels returned to baseline, then decreased after DRS was turned off (5.17  $\pm$  0.45,  $p < 0.01$ ). These findings were congruous with those observed for DCS, consistent with a common mode of A $\beta$ -fiber activation.

### Superficial dorsal horn GABAergic neuron activation by dorsal column stimulation or dorsal root stimulation is independent of neuron depth

We were surprised that DCS and DRS did not elicit sustained activation of SDH inhibitory cells. As low-threshold myelinated A $\beta$ -fiber afferents terminate in the deeper dorsal horn lamina (II–VI), we set to determine whether DCS or DRS drove activity preferentially in deeper SDH.<sup>33</sup> We took advantage of the ability of multiphoton microscopy to image deep in tissues

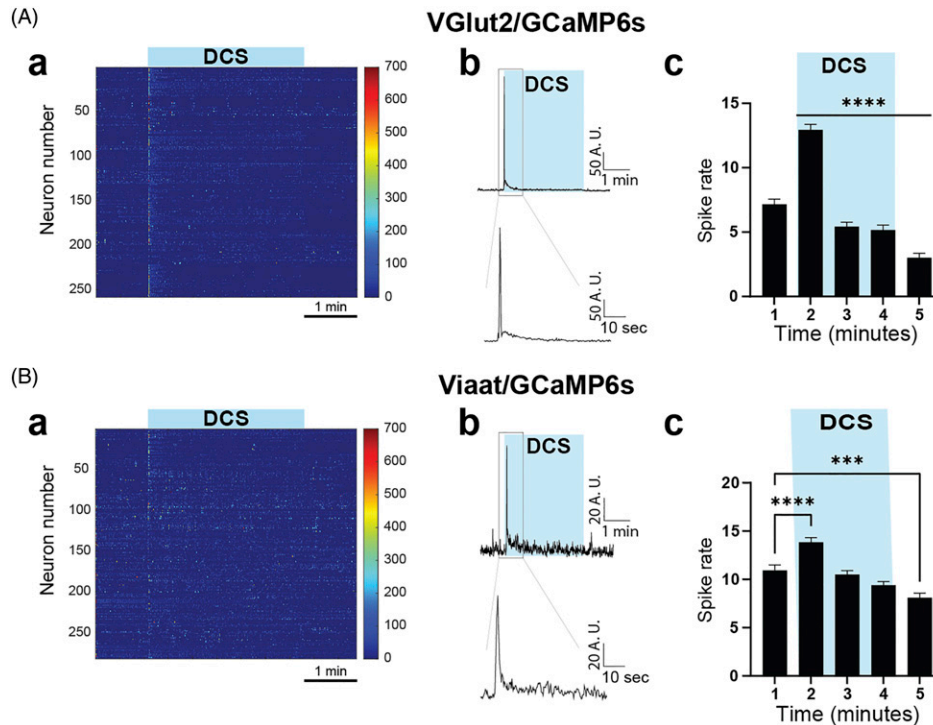


**Figure 3.** Dorsal column stimulation modulates the activity of glutamatergic and GABAergic populations. (Aa) Raster plot of inferred glutamatergic neuronal activity. Two-photon images were acquired for 5 min, and dorsal column stimulation (DCS) was delivered for 3 min, with charge-balanced biphasic pulses at a frequency of 50 Hz and an amplitude of 100  $\mu$ A. The duration of each phase was 0.2 ms; these parameters are similar to those typically used in patients. (Ab) Top panel: Averaged inferred activity for all neurons ( $n = 258$  from five mice). The lower panel demonstrates activity over a 60 s time window. (Ac) Neuronal activity was binned every minute. Activity changed at every time point during and after stimulation (RM ANOVA  $F(4,253) = 142.90$ ,  $p < 0.0001$ ). Glutamatergic activity significantly increased during the first minute of stimulation, then decreased below baseline and remained depressed once dorsal column stimulation was turned off. (B) DCS transiently increased GABAergic neuronal activity. (Ba) Raster plot of inferred neuronal activity. (Bb) Averaged spike rates in all neurons ( $n = 327$  from six mice; top panel); the lower panel demonstrates activity over a narrower window (60 s long). (Bc) Neuronal activity was binned every minute. Although GABAergic activity increased briefly during the first minute of stimulation, it subsequently returned to baseline. Activity levels decreased below baseline once the stimulation was turned off (RM ANOVA  $F(4,322) = 27.27$ ,  $p < 0.0001$ ).

and examined neurons residing up to 180  $\mu$ m from the surface of the dorsal horn, which corresponds to lamina III.<sup>34,35</sup> We delivered a 30-s train of DCS at six planes separated by 30  $\mu$ m, sampling neurons throughout SDH (Figure 5(a)). We binned neuronal activity for the 30 s of stimulation (Figure 5(b)). The calculated spike rates were higher than those described above (e.g., Figures 3 and 4) due to the shorter duration of stimulation over which the responses were binned. There were no effects of depth on GABAergic neuronal activity for both DCS or DRS via ANOVA. These findings suggest that DCS or DRS did not preferentially activate inhibitory neurons residing in deeper SDH.

#### *Dorsal column stimulation and dorsal root stimulation drove sustained activation of a subset of GABAergic neurons*

The experiments thus far examined pooled activity in the entire population of glutamatergic and GABAergic neurons. However, some neurons increased their activity briskly at the onset of stimulation. We, therefore, aimed to determine if the

effects of continuous A $\beta$ -fiber stimulation were different in neurons classified based on their initial responses. To this end, we defined neurons as responders, characterized by a 50% increase in activity during the first 10 s of DCS or DRS, or non-responders. We observed a significant difference in the fraction of responders between glutamatergic and GABAergic populations (Figure 6(a)), with both locations of stimulation preferentially driving a more substantial proportion of glutamatergic neurons (84% vs 52% for DCS, 76% vs 59% for DRS;  $p < 0.001$ ). Glutamatergic responders showed a significant increase during the first minute of DCS; activity levels then decreased below baseline, despite ongoing stimulation (Figure 6(b) left panel). GABAergic responders exhibited a different pattern of activity during DCS or DRS: an initial robust response, followed by significantly elevated activity levels for the entire duration of the stimulation, and finally a return to baseline levels once the stimulation stopped (Figure 6(b) right panel). As only about half of GABAergic neurons were responders, we also examined non-responders. Notably, GABAergic non-responders had

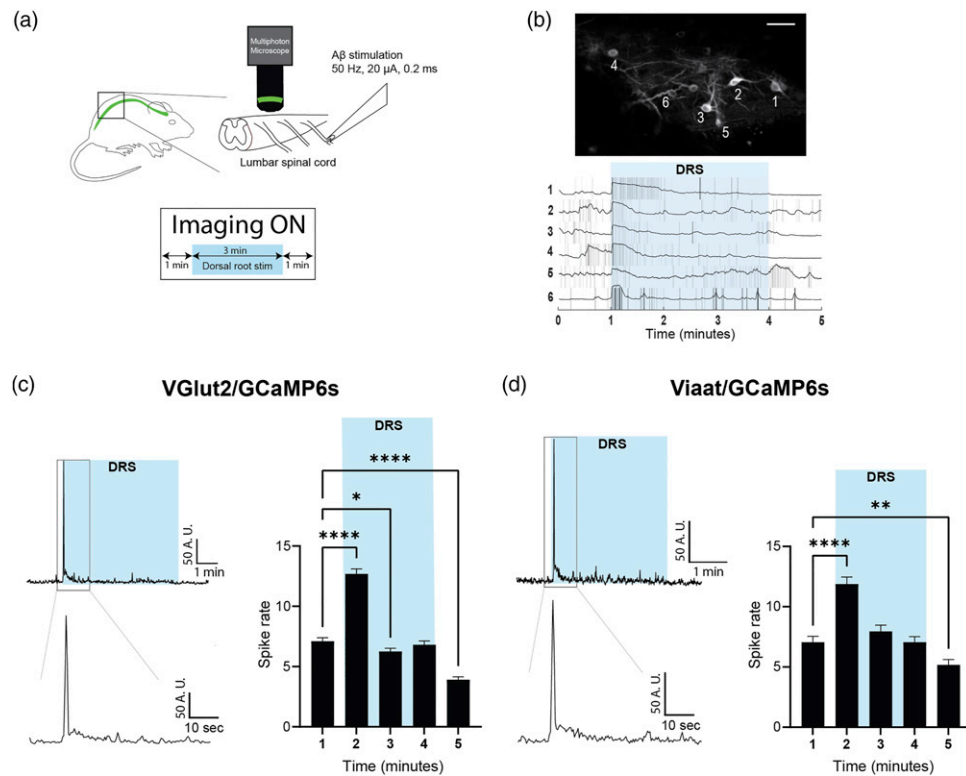


**Figure 4.** Dorsal root stimulation at A $\beta$ -fiber intensity modulates the activity of glutamatergic and GABAergic populations. (a) Experimental setup. Dorsal root stimulation (DRS) (3 min at 50 Hz, 20  $\mu$ A, 0.2 ms) was delivered using a suction pipette, and superficial dorsal horn neurons were imaged one segment rostral. (b) Max projected image of an exemplar time-series stack obtained in a VGLut2/GCaMP6s mouse imaged over 5 min. Lower panel: Raw fluorescence traces (darker lines; individually scaled; corresponding to the numbers in the image) overlaid on inferred spiking. Scale bar 50  $\mu$ m. (c) Averaged inferred activity in all glutamatergic neurons ( $n = 475$  from six mice; upper left panel). The lower panel shows a narrower time window (60 s long). Neuronal activity was binned every minute (right panel). Activity levels increased immediately after stimulation, then decreased below baseline during the second minute and after the stimulation ended (RM ANOVA  $F(4,471) = 180.80$ ). (d) Averaged inferred activity in all GABAergic neurons ( $n = 184$  from six mice; upper left panel). The lower panel includes a narrower time window. Neuronal activity was binned every minute (right panel). Activity levels increased immediately after stimulation and decreased below baseline after the stimulation was stopped (RM ANOVA  $F(4,179) = 40.79$ ).

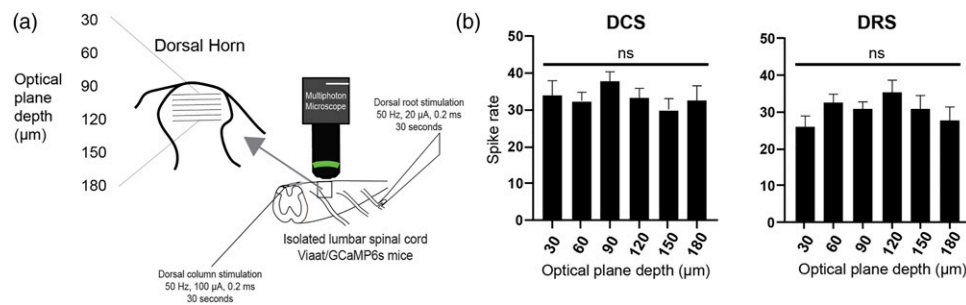


**Figure 5.** Superficial dorsal horn GABAergic neuron activity evoked by dorsal column and dorsal root stimulation is independent of depth. (a) The activity of GABAergic neurons was measured up to 180  $\mu$ m below the surface of the dorsal horn during a 30-s long train of dorsal column (DCS) or dorsal root stimulation (DRS). Optical planes were imaged in 30  $\mu$ m increments. (b) Averaged activity during stimulation (30 s) was plotted over depth. There was no significant effect of depth on DCS-evoked activity (one-way ANOVA  $F(5, 406) = 0.96$ ,  $p = 0.44$ ;  $n = \sim 68$  neurons/plane from nine mice). Similarly, there was no effect of depth on responses evoked by dorsal root stimulation ( $F(5, 331) = 1.28$ ,  $p = 0.27$ ;  $n = \sim 56$  neurons/plane from 10 mice).

increased baseline activity levels versus responders (inferred spike rate:  $13.99 \pm 0.92$  vs  $7.17 \pm 0.66$  for DCS,  $10.44 \pm 0.79$  vs  $4.82 \pm 0.52$  for DRS, in non-responders and responders,

respectively,  $p < 0.0001$  for both conditions). The activity levels of non-responders decreased below baseline during and after stimulation (Figure 6(c)). Therefore, our findings

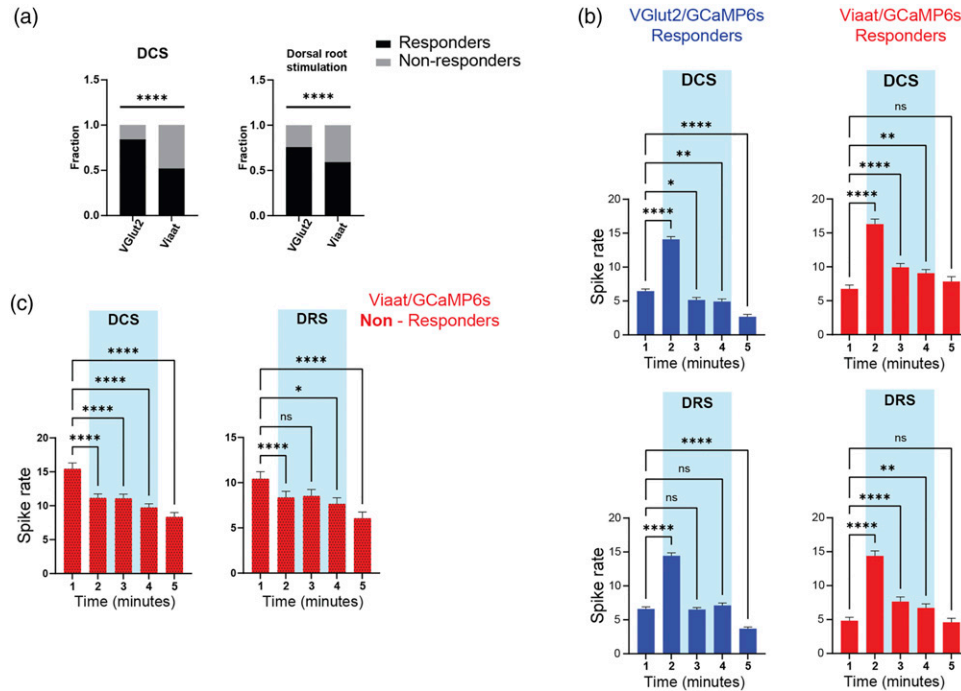


**Figure 6.** Dorsal column and dorsal root stimulation increased firing in a subset of GABAergic neurons. (a) Responder neurons were defined by an increase in spike rates of >50% during the first 10 s after the stimulation was turned on. Both dorsal column (DCS) and dorsal root stimulation (DRS) activated a more significant proportion of glutamatergic neurons ( $p < 0.0001$  for both). (b) DCS or DRS preferentially increased activity in GABAergic responders. Glutamatergic responders had increased activity levels during the first minute of stimulation, followed by a decrease below baseline during and after stimulation ( $n = 217$  neurons from five mice; RM ANOVA  $F(4, 212) = 196.2$  followed by Dunnett's multiple comparisons test,  $p < 0.0001$ ). In contrast, GABAergic responders had elevated firing rates for the entire duration of DCS and returned to baseline levels once the stimulation was turned off ( $n = 170$  neurons from six mice; RM ANOVA  $F(4, 165) = 49.51$ ,  $p < 0.0001$ ). Lower panels: Glutamatergic neurons increased their activity initially once DRS began, then spike rates returned to baseline. Activity levels decreased from baseline once the stimulation was turned off ( $n = 360$  neurons from six mice; RM ANOVA  $F(4, 355) = 224.0$ ,  $p < 0.0001$ ). As observed with DCS, GABAergic responder activity was potentiated for the entire duration of stimulation and then returned to baseline ( $n = 109$  neurons from six mice; RM ANOVA  $F(4, 104) = 65.71$ ,  $p < 0.0001$ ). (c) Non-responder GABAergic neurons had depressed activity levels during and after stimulation for both DCS or DRS (DCS  $n = 157$  from six mice, RM ANOVA  $F(4, 152) = 22.01$ ,  $p < 0.0001$ ; dorsal root stimulation  $n = 74$  neurons from six mice, RM ANOVA  $F(4, 69) = 8.978$ ,  $p < 0.001$ ).

suggest the existence of two populations of GABAergic neurons with dichotomous responses to A $\beta$ -fiber stimulation.

## Discussion

We imaged the activity of molecularly defined glutamatergic and GABAergic SDH neurons *in vitro* and found that DCS and DRS induced biphasic responses in both populations. We observed a robust but transient initial activation at the start of stimulation, followed by depressed activity levels in glutamatergic neurons, and return to baseline in GABAergic cells. Both populations showed slightly depressed activity levels after the stimulation was turned off. Although most glutamatergic neurons responded transiently to stimulation, only about half of GABAergic neurons responded either to DCS or DRS. GABAergic responders had significantly increased activity levels during the entire duration of stimulation; in

contrast, non-responders displayed depressed levels. To our knowledge, this is the first report supporting the existence of a subset of GABAergic neurons engaged by sustained A $\beta$ -fiber activation, as proposed in GCT.<sup>1</sup>

Recent studies highlighted the cellular heterogeneity of the dorsal horn, including the presence of functionally distinct circuits involved in mechanical pain and itch.<sup>36,37</sup> Inhibitory neurons are particularly relevant for gating afferent excitatory inputs and have been implicated in chronic pain conditions.<sup>38,39</sup> Five non-overlapping populations of inhibitory interneurons were described in SDH, the largest proportion (1/3) being neuropeptide Y expressing cells.<sup>40</sup> In our experiments, about half of GABAergic neurons were classified as responders to DCS or DRS, suggesting that more than one population was activated. Non-responders had nearly double baseline (spontaneous) activity levels than responders, implying that they may represent a distinct



physiological subset. Notably, responders maintained elevated activity levels during stimulation (Figure 6). Thus, we provide direct evidence that DCS and DRS augmented the activity of a subset of GABAergic neurons residing in SDH, which may explain how A $\beta$ -fiber stimulation increases GABA release,<sup>4,5</sup> reverses wide dynamic range neuron (WDR) plasticity,<sup>41</sup> and depresses WDR neuron hyperexcitability.<sup>29</sup> As over 30 molecularly defined populations of SDH neurons have recently been described, future experiments will be needed to investigate the identity of GABAergic responders and whether they are necessary for generating pain relief.<sup>10,11</sup>

Prior studies investigated which neurons are modulated by A $\beta$ -fiber stimulation by examining the expression of immediate early genes and found modest<sup>7</sup> or no<sup>42</sup> increases in the number of immunoreactive cells for DCS at 50–60 Hz. We found robust activation in most SDH neurons that lasted only seconds, which may be insufficient to drive expression of immediate early genes,<sup>43,44</sup> and could explain prior reports. The mechanism for the brief activation deserves further investigation. One possibility is neurotransmitter depletion, as previously described for continuous A $\beta$ -fiber stimulation.<sup>15,45</sup> Alternatively, it may be that the subset of GABAergic responders caused widespread inhibition of other SDH populations. As A $\beta$ -fibers terminate in the inner dorsal horn, it is possible that deeper GABAergic neurons (e.g. lamina III–VI) receive stronger inputs and are engaged differently during stimulation.<sup>46</sup> For example, parvalbumin-expressing interneurons reside in lamina II/III and receive direct inputs from myelinated afferents; in turn, they drive presynaptic and postsynaptic inhibition of lamina II excitatory neurons.<sup>15</sup> We tested this hypothesis within the constraints of our imaging system and found comparable responses to DCS or DRS in cells residing up to 180  $\mu$ m below the surface, which corresponds to lamina III. Future experiments using novel microscopy techniques capable of imaging deeper in biological tissues, such as 3-photon microscopy, are needed.<sup>47</sup>

In our study, DCS and DRS evoked responses in both glutamatergic and GABAergic SDH neurons. We found a higher percentage of responsive glutamatergic neurons compared to what was reported before.<sup>48–50</sup> These differences are likely due to our approach (intact spinal cord) and the use of a sustained train of A $\beta$ -fiber stimulation versus single pulses. Recently, it was proposed that DCS directly excites superficial dorsal horn dendrites.<sup>2</sup> We do not expect this mechanism in our preparation as the regions imaged were more than one segment distal to the electrode, further than the previously reported rostro-caudal dendritic arbor dimensions for SDH neurons.<sup>51</sup> Moreover, similar levels of activation were seen with DRS. Earlier work *in vivo* described excitatory synaptic drive from collaterals of dorsal column fibers into lamina I–III.<sup>6</sup> In that study, 24 of 29 recorded units showed excitation after brief DCS (1-s train at 50 Hz), with shorter latencies in neurons residing in lamina II–III. The

authors concluded that the neurons activated were inhibitory cells (given the inhibitory nature of DCS), although the identity of the recorded neurons was not investigated. A recent study found that projection neurons responded heterogeneously to DCS, suggesting complex circuit interactions, although the stimulation duration was also brief.<sup>52</sup> As we observed biphasic responses, it will be critical for future studies to determine the effects of sustained A $\beta$ -fiber stimulation on SDH output projection neurons.

An unexpected finding was that DCS and DRS strongly activated glutamatergic SDH neurons. Clinically, tonic DCS elicits sensory responses termed paresthesias. Electrodes are placed such that paresthesias overlap the painful body regions, which is necessary for pain relief.<sup>27</sup> Although paresthesias have been long believed to represent activation of dorsal column fibers,<sup>27,29,53</sup> our findings suggest that they could also signify retrograde activation of excitatory SDH networks, an off-target effect. This could explain why most patients find paresthesias unpleasant and why stimulation amplitude windows tend to be narrow.<sup>54</sup> These observations have prompted strategies to minimize paresthesias, including sensors that adapt stimulation intensity to patient position,<sup>55</sup> and closed-loop stimulation, with improved pain relief.<sup>56</sup> Furthermore, paresthesia-free stimulation paradigms have been successfully implemented.<sup>57–60</sup> It will be critical to examine the frequency- and waveform-dependent activation of SDH neurons, particularly in models of chronic pain, where neuropathy-related changes have been demonstrated.<sup>39</sup> It is tempting to speculate that specific frequencies and waveforms differentially activate glutamatergic and GABAergic populations depending on the type of pain, although this hypothesis needs further attention.

Various approaches have been used to identify physiological A $\beta$ -fiber stimulation parameters *in vitro*,<sup>29,30</sup> as overstimulation could result in unwanted recruitment of non-dorsal column neuropil (such as dorsal root entry zone axons and/or adjacent dendritic arbors) and A $\delta$ /C-fibers for DCS and DRS, respectively. Although DRS pulse widths and amplitudes selective for A $\beta$ -fibers have been described in mice,<sup>30,48</sup> this information is not available for DCS. We addressed this by identifying stimulation parameters *in vivo*, using a miniaturized bipolar electrode and charge-balanced pulses, which parallels clinical practice. We measured motor thresholds and confirmed dorsal column activation by measuring retrogradely conducted compound action potentials *in vivo*. Activation of A $\beta$ -fibers was observed *in vitro* at the lumbar dorsal roots, using a similar configuration as in our imaging experiments. In previous mouse studies, a single epidural cathode electrode was used for DCS, with the anode placed in the abdomen.<sup>61</sup> The average motor threshold amplitude reported in that study was 730  $\mu$ A, which is an order of magnitude greater than what we measured (71  $\mu$ A). We attribute this discrepancy to the bipolar architecture of our

electrode, resulting in more focal electrical fields and greater activation of dorsal column axons while minimizing unwanted heat generation and electrolysis.<sup>28,62</sup> Studies in rats, using larger electrodes, reported motor and dorsal column axon thresholds comparable to ours, confirming the scalability of our design.<sup>29,63,64</sup> These results validate the usefulness of our electrode to study the mechanisms of DCS in mice.<sup>65</sup>

Multiphoton microscopy of GCaMP has been used extensively to understand the behavior of neuronal circuits.<sup>66,67</sup> The mouse spinal cord is well-suited for optical techniques given its size and expanding understanding of the molecularly defined populations processing somatosensation.<sup>19,68,69</sup> We imaged activity-evoked changes in intracellular calcium using GCaMP6s and deconvolved activity using spike-inference algorithms built into the software CaImAn, an established methodology.<sup>24,26,70</sup> A recent imaging study demonstrated that calcium responses faithfully encode action potentials in lamina I in mice.<sup>71</sup> Others have found that a significant proportion of single action potentials are missed by GCaMP6 imaging, suggesting that our results may underrepresent the spontaneous activity of SDH populations.<sup>72</sup> Future studies will be required to collect ground-truth electrophysiological and imaging data in spinal cord populations, as done in other regions.<sup>73</sup> This information will be critical for optimizing spike detection algorithms.

In summary, we provide evidence that DCS and DRS at a clinically relevant frequency and physiological amplitudes activate and modulate the activity of SDH neurons and drive sustained firing in a subset of GABAergic cells—as proposed in GCT. Future studies are needed to characterize the molecular identity of GABAergic responders and whether their activation is necessary for analgesic effects. The optimization and implementation of neuromodulation therapies will depend on a detailed understanding of the effects of A $\beta$ -fiber stimulation on spinal cord circuits.

### Declaration of Conflicting Interests

The author(s) declared no potential conflicts of interest with respect to the research, authorship, and/or publication of this article.

### Funding

The author(s) disclosed receipt of the following financial support for the research, authorship, and/or publication of this article: This work was supported by the National Institutes of Health (grant K08NS099503 to ADS).

### Data availability statement

The data that support the findings of this study are available in electronic format from the corresponding author, ADS, upon reasonable request.

### ORCID iD

Andrei D Sdrulla  <https://orcid.org/0000-0002-4152-8405>

### References

- Melzack R, Wall PD. Pain mechanisms: a new theory. *Science* 1965; 150: 971–979. DOI: [10.1126/science.150.3699.971](https://doi.org/10.1126/science.150.3699.971).
- Jensen MP, Brownstone RM. Mechanisms of spinal cord stimulation for the treatment of pain: still in the dark after 50 years. *Eur J Pain* 2019; 23: 652–659. DOI: [10.1002/ejp.1336](https://doi.org/10.1002/ejp.1336).
- Lesperance LS, Lankarany M, Zhang TC, Esteller R, Ratté S, Prescott SA. Artfactual hyperpolarization during extracellular electrical stimulation: proposed mechanism of high-rate neuromodulation disproved. *Brain Stimul* 2018; 11: 582–591, DOI: [10.1016/j.brs.2017.12.004](https://doi.org/10.1016/j.brs.2017.12.004).
- Cui JG, O'Connor WT, Ungerstedt U, Linderöth B, Meyerson BA. Spinal cord stimulation attenuates augmented dorsal horn release of excitatory amino acids in mononeuropathy via a GABAergic mechanism. *Pain* 1997; 73: 87–95. DOI: [10.1016/s0304-3959\(97\)00077-8](https://doi.org/10.1016/s0304-3959(97)00077-8).
- Meuwissen KPV, de Vries LE, Gu JW, Zhang TC, Joosten EAJ. Burst and tonic spinal cord stimulation both activate spinal GABAergic mechanisms to attenuate pain in a rat model of chronic neuropathic pain. *Pain Pract* 2020; 20: 75–87. DOI: [10.1111/papr.12831](https://doi.org/10.1111/papr.12831).
- Dubuisson D. Effect of dorsal-column stimulation on gelatinosa and marginal neurons of cat spinal cord. *J Neurosurg* 1989; 70: 257–265. DOI: [10.3171/jns.1989.70.2.0257](https://doi.org/10.3171/jns.1989.70.2.0257).
- Smits H, Kleef MV, Honig W, Gerver J, Gobrecht P, Joosten EAJ. Spinal cord stimulation induces c-fos expression in the dorsal horn in rats with neuropathic pain after partial sciatic nerve injury. *Neurosci Lett* 2009; 450: 70–73, DOI: [10.1016/j.neulet.2008.11.013](https://doi.org/10.1016/j.neulet.2008.11.013).
- Li S, Ye F, Farber JP, Linderöth B, Zhang T, Gu JW, Moffitt M, Garrett K, Chen J, Foreman RD. Dependence of c-fos expression on amplitude of high-frequency spinal cord stimulation in a rodent model. *Neuromodulation* 2019; 22: 172–178, DOI: [10.1111/ner.12852](https://doi.org/10.1111/ner.12852).
- Maeda Y, Ikeuchi M, Wacnik P, Sluka KA. Increased c-fos immunoreactivity in the spinal cord and brain following spinal cord stimulation is frequency-dependent. *Brain Res* 2009; 1259: 40–50. DOI: [10.1016/j.brainres.2008.12.060](https://doi.org/10.1016/j.brainres.2008.12.060).
- Häring M, Zeisel A, Hochgerner H, Rinwa P, Jakobsson JET, Lönnerberg P, La Manno G, Sharma N, Borgius L, Kiehn O, Lagerström MC, Linnarsson S, Ernfors P. Neuronal atlas of the dorsal horn defines its architecture and links sensory input to transcriptional cell types. *Nat Neurosci* 2018; 21: 869–880. DOI: [10.1038/s41593-018-0141-1](https://doi.org/10.1038/s41593-018-0141-1).
- Sathyamurthy A, Johnson KR, Matson KJE, Dobrott CI, Li L, Ryba AR, Bergman TB, Kelly MC, Kelley MW, Levine AJ. Massively parallel single nucleus transcriptional profiling defines spinal cord neurons and their activity during behavior. *Cel Reports* 2018; 22: 2216–2225. DOI: [10.1016/j.celrep.2018.02.003](https://doi.org/10.1016/j.celrep.2018.02.003).
- Todd AJ. Identifying functional populations among the interneurons in laminae I–III of the spinal dorsal horn. *Mol Pain* 2017; 13: 1744806917693003. DOI: [10.1177/1744806917693003](https://doi.org/10.1177/1744806917693003).
- Petitjean H, Pawlowski SA, Fraine SL, Sharif B, Hamad D, Fatima T, Berg J, Brown CM, Jan LY, Ribeiro-da-Silva A, Braz JM, Basbaum AI, Sharif-Naeini R. Dorsal horn parvalbumin

- neurons are gate-keepers of touch-evoked pain after nerve injury. *Cell Rep* 2015; 13: 1246–1257. DOI: [10.1016/j.celrep.2015.09.080](https://doi.org/10.1016/j.celrep.2015.09.080).
14. Torsney C, MacDermott AB. Disinhibition opens the gate to pathological pain signaling in superficial neurokinin 1 receptor-expressing neurons in rat spinal cord. *J Neurosci* 2006; 26: 1833–1843. DOI: [10.1523/JNEUROSCI.4584-05.2006](https://doi.org/10.1523/JNEUROSCI.4584-05.2006).
  15. Boyle KA, Gradwell MA, Yasaka T, Dickie AC, Polgár E, Ganley RP, Orr DPH, Watanabe M, Abaira VE, Kuehn ED, Zimmerman AL, Ginty DD, Callister RJ, Graham BA, Hughes DI. Defining a spinal microcircuit that gates myelinated afferent input: implications for tactile allodynia. *Cell Rep* 2019; 28: 526–540.e6, DOI: [10.1016/j.celrep.2019.06.040](https://doi.org/10.1016/j.celrep.2019.06.040).
  16. Grienberger C, Konnerth A. Imaging calcium in neurons. *Neuron* 2012; 73: 862–885. DOI: [10.1016/j.neuron.2012.02.011](https://doi.org/10.1016/j.neuron.2012.02.011).
  17. Emiliani V, Cohen AE, Deisseroth K, Hausser M. All-optical interrogation of neural circuits. *J Neurosci* 2015; 35: 13917–13926. DOI: [10.1523/JNEUROSCI.2916-15.2015](https://doi.org/10.1523/JNEUROSCI.2916-15.2015).
  18. Xu Q, Dong X. Calcium imaging approaches in investigation of pain mechanism in the spinal cord. *Exp Neurol* 2019; 317: 129–132, DOI: [10.1016/j.expneurol.2019.03.002](https://doi.org/10.1016/j.expneurol.2019.03.002).
  19. Harding EK, Fung SW, Bonin RP. Insights into spinal dorsal horn circuit function and dysfunction using optical approaches. *Front Neural Circuits* 2020; 14: 31. DOI: [10.3389/fncir.2020.00031](https://doi.org/10.3389/fncir.2020.00031).
  20. Chen TW, Wardill TJ, Sun Y, Pulver SR, Renninger SL, Baohan A, Schreiter ER, Kerr RA, Orger MB, Jayaraman V, Looger LL, Svoboda K, Kim DS. Ultrasensitive fluorescent proteins for imaging neuronal activity. *Nature* 2013; 499: 295–300. DOI: [10.1038/nature12354](https://doi.org/10.1038/nature12354).
  21. Fan W, Sdrulla AD. Differential modulation of excitatory and inhibitory populations of superficial dorsal horn neurons in lumbar spinal cord by A $\beta$ -fiber electrical stimulation. *Pain* 2020; 161: 1650–1660. DOI: [10.1097/j.pain.0000000000001836](https://doi.org/10.1097/j.pain.0000000000001836).
  22. Safronov BV, Pinto V, Derkach VA. High-resolution single-cell imaging for functional studies in the whole brain and spinal cord and thick tissue blocks using light-emitting diode illumination. *J Neurosci Methods* 2007; 164: 292–298. DOI: [10.1016/j.jneumeth.2007.05.010](https://doi.org/10.1016/j.jneumeth.2007.05.010).
  23. Chisholm KI, Lo Re L, Polgár E, Gutierrez-Mecinas M, Todd AJ, McMahon SB. The encoding of cutaneous stimuli by lamina I projection neurons. *Pain* 2021; 162: 2405–2417. DOI: [10.1097/j.pain.0000000000002226](https://doi.org/10.1097/j.pain.0000000000002226).
  24. Giovannucci A, Friedrich J, Gunn P, Kalfon J, Brown BL, Koay SA, Taxis J, Najafi F, Gauthier JL, Zhou P, Khakh BS, Tank DW, Chklovskii DB, Pnevmatikakis EA. CalMan an open source tool for scalable calcium imaging data analysis. *Elife* 2019; 8: e38173. DOI: [10.7554/eLife.38173](https://doi.org/10.7554/eLife.38173).
  25. Pnevmatikakis EA, Giovannucci A. NoRMCorre: an online algorithm for piecewise rigid motion correction of calcium imaging data. *J Neurosci Methods* 2017; 291: 83–94. DOI: [10.1016/j.jneumeth.2017.07.031](https://doi.org/10.1016/j.jneumeth.2017.07.031).
  26. Pnevmatikakis EA, Soudry D, Gao Y, Machado TA, Merel J, Pfau D, Reardon T, Mu Y, Lacefield C, Yang W, Ahrens M, Bruno R, Jessell TM, Peterka DS, Yuste R, Paninski L. Simultaneous denoising, deconvolution, and demixing of calcium imaging data. *Neuron* 2016; 89: 285–299. DOI: [10.1016/j.neuron.2015.11.037](https://doi.org/10.1016/j.neuron.2015.11.037).
  27. North RB, Kidd DH, Zahurak M, James CS, Long DM. Spinal cord stimulation for chronic, intractable pain: experience over two decades. *Neurosurgery* 1993; 32: 384–395. DOI: [10.1227/00006123-199303000-00008](https://doi.org/10.1227/00006123-199303000-00008).
  28. Miller JP, Eldabe S, Buchser E, Johaneck LM, Guan Y, Linderroth B. Parameters of spinal cord stimulation and their role in electrical charge delivery: a review. *Neuromodulation* 2016; 19: 373–384. DOI: [10.1111/ner.12438](https://doi.org/10.1111/ner.12438).
  29. Guan Y, Wacnik PW, Yang F, Carteret AF, Chung CY, Meyer RA, Raja SN. Spinal cord stimulation-induced analgesia: electrical stimulation of dorsal column and dorsal roots attenuates dorsal horn neuronal excitability in neuropathic rats. *Anesthesiology* 2010; 113: 1392–1405. DOI: [10.1097/ALN.0b013e3181fcd95c](https://doi.org/10.1097/ALN.0b013e3181fcd95c).
  30. Sdrulla AD, Xu Q, He SQ, Tiwari V, Yang F, Zhang C, Shu B, Shechter R, Raja SN, Wang Y, Dong X, Guan Y. Electrical stimulation of low-threshold afferent fibers induces a prolonged synaptic depression in lamina II dorsal horn neurons to high-threshold afferent inputs in mice. *Pain* 2015; 156: 1008–1017. DOI: [10.1097/01.j.pain.0000460353.15460.a3](https://doi.org/10.1097/01.j.pain.0000460353.15460.a3).
  31. Yang F, Xu Q, Cheong YK, Shechter R, Sdrulla A, He SQ, Tiwari V, Dong X, Wacnik PW, Meyer R, Raja SN, Guan Y. Comparison of intensity-dependent inhibition of spinal wide-dynamic range neurons by dorsal column and peripheral nerve stimulation in a rat model of neuropathic pain. *Eur J Pain* 2014; 18: 978–988. DOI: [10.1002/j.1532-2149.2013.00443.x](https://doi.org/10.1002/j.1532-2149.2013.00443.x).
  32. Yang F, Xu Q, Shu B, Tiwari V, He SQ, Vera-Portocarrero LP, Dong X, Linderroth B, Raja SN, Wang Y, Guan Y. Activation of cannabinoid CB1 receptor contributes to suppression of spinal nociceptive transmission and inhibition of mechanical hypersensitivity by A $\beta$ -fiber stimulation. *Pain* 2016; 157: 2582–2593. DOI: [10.1097/j.pain.0000000000000680](https://doi.org/10.1097/j.pain.0000000000000680).
  33. Todd AJ. Neuronal circuitry for pain processing in the dorsal horn. *Nat Rev Neurosci* 2010; 11: 823–836. DOI: [10.1038/nrn294710.1038/nrn2947](https://doi.org/10.1038/nrn294710.1038/nrn2947).
  34. Martin WJ, Malmberg AB, Basbaum AI. PKC $\gamma$  contributes to a subset of the NMDA-dependent spinal circuits that underlie injury-induced persistent pain. *J Neurosci* 2001; 21: 5321–5327.
  35. *Allen spinal cord Atlas*, <https://mousespinal.brain-map.org/> (2009, accessed 2 24 2021).
  36. Chen XJ, Sun YG. Central circuit mechanisms of itch. *Nat Commun* 2020; 11: 3052. DOI: [10.1038/s41467-020-16859-5](https://doi.org/10.1038/s41467-020-16859-5).
  37. Peirs C, Dallel R, Todd AJ. Recent advances in our understanding of the organization of dorsal horn neuron populations and their contribution to cutaneous mechanical allodynia. *J Neural Transm (Vienna)* 2020; 127: 505–525. DOI: [10.1007/s00702-020-02159-1](https://doi.org/10.1007/s00702-020-02159-1).
  38. Stachowski NJ, Dougherty KJ. Spinal inhibitory interneurons: gatekeepers of sensorimotor pathways. *Int J Mol Sci* 2021; 22: 2667. DOI: [10.3390/ijms22052667](https://doi.org/10.3390/ijms22052667).
  39. Moore KA, Kohno T, Karchewski LA, Scholz J, Baba H, Woolf CJ. Partial peripheral nerve injury promotes a selective loss of

- GABAergic inhibition in the superficial dorsal horn of the spinal cord. *J Neurosci* 2002; 22: 6724–6731. DOI: [10.1523/jneurosci.22-15-06724.2002](https://doi.org/10.1523/jneurosci.22-15-06724.2002).
40. Boyle KA, Gutierrez-Mecinas M, Polgár E, Mooney N, O'Connor E, Furuta T, Watanabe M, Todd AJ. A quantitative study of neurochemically defined populations of inhibitory interneurons in the superficial dorsal horn of the mouse spinal cord. *Neuroscience* 2017; 363: 120–133. DOI: [10.1016/j.neuroscience.2017.08.044](https://doi.org/10.1016/j.neuroscience.2017.08.044).
  41. Wallin J, Fiska A, Tjolsen A, Linderorth B, Hole K. Spinal cord stimulation inhibits long-term potentiation of spinal wide dynamic range neurons. *Brain Res* 2003; 973: 39–43.
  42. Maeda Y, Wacnik PW, Sluka KA. Low frequencies, but not high frequencies of bi-polar spinal cord stimulation reduce cutaneous and muscle hyperalgesia induced by nerve injury. *Pain* 2008; 138: 143–152. DOI: [10.1016/j.pain.2007.11.016](https://doi.org/10.1016/j.pain.2007.11.016).
  43. Hunt SP, Pini A, Evan G. Induction of c-fos-like protein in spinal cord neurons following sensory stimulation. *Nature* 1987; 328: 632–634. DOI: [10.1038/328632a0](https://doi.org/10.1038/328632a0).
  44. Molander C, Hongpaisan J, Persson JK. Distribution of c-fos expressing dorsal horn neurons after electrical stimulation of low threshold sensory fibers in the chronically injured sciatic nerve. *Brain Res* 1994; 644: 74–82. DOI: [10.1016/0006-8993\(94\)90349-2](https://doi.org/10.1016/0006-8993(94)90349-2).
  45. Cheng L, Duan B, Huang T, Zhang Y, Chen Y, Britz O, Garcia-Campmany L, Ren X, Vong L, Lowell BB, Goulding M, Wang Y, Ma Q. Identification of spinal circuits involved in touch-evoked dynamic mechanical pain. *Nat Neurosci* 2017; 20: 804–814. DOI: [10.1038/nn.4549](https://doi.org/10.1038/nn.4549).
  46. Zeilhofer HU, Wildner H, Yévenes GE. Fast synaptic inhibition in spinal sensory processing and pain control. *Physiol Rev* 2012; 92: 193–235. DOI: [10.1152/physrev.00043.2010](https://doi.org/10.1152/physrev.00043.2010).
  47. Takasaki K, Abbasi-Asl R, Waters J. Superficial bound of the depth limit of two-photon imaging in mouse brain. *eNeuro* 2020; 7: ENEURO.0255–19.2019. DOI: [10.1523/eneuro.0255-19.2019](https://doi.org/10.1523/eneuro.0255-19.2019).
  48. Daniele CA, MacDermott AB. Low-threshold primary afferent drive onto GABAergic interneurons in the superficial dorsal horn of the mouse. *J Neurosci* 2009; 29: 686–695. DOI: [10.1523/JNEUROSCI.5120-08.2009](https://doi.org/10.1523/JNEUROSCI.5120-08.2009).
  49. Duan B, Cheng L, Bourane S, Britz O, Padilla C, Garcia-Campmany L, Krashes M, Knowlton W, Velasquez T, Ren X, Ross SE, Lowell BB, Wang Y, Goulding M, Ma Q. Identification of spinal circuits transmitting and gating mechanical pain. *Cell* 2014; 159: 1417–1432. DOI: [10.1016/j.cell.2014.11.003](https://doi.org/10.1016/j.cell.2014.11.003).
  50. Zhang Y, Liu S, Zhang Y-Q, Goulding M, Wang Y-Q, Ma Q. Timing mechanisms underlying gate control by feedforward inhibition. *Neuron* 2018; 99: 941–955.e944, DOI: [10.1016/j.neuron.2018.07.026](https://doi.org/10.1016/j.neuron.2018.07.026).
  51. Grudt TJ, Perl ER. Correlations between neuronal morphology and electrophysiological features in the rodent superficial dorsal horn. *J Physiol* 2002; 540: 189–207. DOI: [10.1113/jphysiol.2001.012890](https://doi.org/10.1113/jphysiol.2001.012890).
  52. Zhang TC, Janik JJ, Peters RV, Chen G, Ji RR, Grill WM. Spinal sensory projection neuron responses to spinal cord stimulation are mediated by circuits beyond gate control. *J Neurophysiol* 2015; 114: 284–300. DOI: [10.1152/jn.00147.2015](https://doi.org/10.1152/jn.00147.2015).
  53. Meyerson BA, Linderorth B. Mode of action of spinal cord stimulation in neuropathic pain. *J Pain Symptom Manag* 2006; 31: S6–S12.
  54. Parker J, Karantonis D, Single P. Hypothesis for the mechanism of action of ECAP-controlled closed-loop systems for spinal cord stimulation. *Health Technol Lett* 2020; 7: 76–80. DOI: [10.1049/htl.2019.0110](https://doi.org/10.1049/htl.2019.0110).
  55. Schultz DM, Webster L, Kosek P, Dar U, Tan Y, Sun M. Sensor-driven position-adaptive spinal cord stimulation for chronic pain. *Pain Physician* 2012; 15: 1–12.
  56. Mekhail N, Levy RM, Deer TR, Kapural L, Li S, Amirdelfan K, Hunter CW, Rosen SM, Costandi SJ, Falowski SM, Burgher AH, Pope JE, Gilmore CA, Qureshi FA, Staats PS, Scowcroft J, Carlson J, Kim CK, Yang MI, Stauss T, Poree L, Brounstein D., Gorman R., Gmel G. E., Hanson E., Karantonis D. M., Khurram A., Kiefer D., Leitner A., Mugañ D., Obradovic M., Parker J., Single P., Soliday N.. Long-term safety and efficacy of closed-loop spinal cord stimulation to treat chronic back and leg pain (Evoke): a double-blind, randomised, controlled trial. *Lancet Neurol* 2020; 19: 123–134. DOI: [10.1016/s1474-4422\(19\)30414-4](https://doi.org/10.1016/s1474-4422(19)30414-4).
  57. North J, Loudermilk E, Lee A, Sachdeva H, Kaiasfas D, Washabaugh E, Sheth S, Scowcroft J, Mekhail N, Lampert B, Yearwood T, Shaw E, Atallah J, McLeod C, Han J, Yu C, Sedrak M, Lucas R, Trobridge A, Hegarty J, Miller N, Chen L, Jain R. Outcomes of a multicenter, prospective, crossover, randomized controlled trial evaluating subperception spinal cord stimulation at  $\leq 1.2$  kHz in previously implanted subjects. *Neuromodulation* 2020; 23: 102–108. DOI: [10.1111/ner.13015](https://doi.org/10.1111/ner.13015).
  58. Kapural L, Yu C, Doust MW, Gliner BE, Vallejo R, Sitzman BT, Amirdelfan K, Morgan DM, Yearwood TL, Bundschu R, Yang T, Benyamin R, Burgher AH. Comparison of 10-kHz high-frequency and traditional low-frequency spinal cord stimulation for the treatment of chronic back and leg pain: 24-month results from a multicenter, randomized, controlled pivotal trial. *Neurosurgery* 2016; 79: 667–677. DOI: [10.1227/neu.0000000000001418](https://doi.org/10.1227/neu.0000000000001418).
  59. Ahmed S, Yearwood T, De Ridder D, Vanneste S. Burst and high frequency stimulation: underlying mechanism of action. *Expert Rev Med Devices* 2018; 15: 61–70. DOI: [10.1080/17434440.2018.1418662](https://doi.org/10.1080/17434440.2018.1418662).
  60. Deer T, Slavin KV, Amirdelfan K, North RB, Burton AW, Yearwood TL, Tavel E, Staats P, Falowski S, Pope J, Justiz R, Fabi AY, Taghva A, Paicius R, Houden T, Wilson D. Success using neuromodulation with BURST (SUNBURST) study: results from a prospective, randomized controlled trial using a novel burst waveform. *Neuromodulation* 2018; 21: 56–66. DOI: [10.1111/ner.12698](https://doi.org/10.1111/ner.12698).
  61. Truin M, van Venrooij P, Duysens V, Deumens R, van Kleef M, Joosten EA. Spinal cord stimulation in a mouse chronic neuropathic pain model. *Neuromodulation* 2007; 10: 358–362. DOI: [10.1111/j.1525-1403.2007.00124.x](https://doi.org/10.1111/j.1525-1403.2007.00124.x).
  62. Cogan SF, Ludwig KA, Welle CG, Takmakov P. Tissue damage thresholds during therapeutic electrical stimulation. *J Neural Eng* 2016; 13: 021001. DOI: [10.1088/1741-2560/13/2/021001](https://doi.org/10.1088/1741-2560/13/2/021001).

63. Chen Z, Huang Q, Yang F, Shi C, Sivanesan E, Liu S, Chen X, Sarma SV, Vera-Portocarrero LP, Linderoth B, Raja SN, Guan Y. The impact of electrical charge delivery on inhibition of mechanical hypersensitivity in nerve-injured rats by sub-sensory threshold spinal cord stimulation. *Neuromodulation* 2019; 22: 163–171. DOI: [10.1111/ner.12910](https://doi.org/10.1111/ner.12910).
64. Yang F, Zhang T, Tiwari V, Shu B, Zhang C, Wang Y, Vera-Portocarrero LP, Raja SN, Guan Y. Effects of combined electrical stimulation of the dorsal column and dorsal roots on wide-dynamic-range neuronal activity in nerve-injured rats. *Neuromodulation* 2015; 18: 592–598. DOI: [10.1111/ner.12341](https://doi.org/10.1111/ner.12341).
65. Gregory NS, Harris AL, Robinson CR, Dougherty PM, Fuchs PN, Sluka KA. An overview of animal models of pain: disease models and outcome measures. *J Pain* 2013; 14: 1255–1269. DOI: [10.1016/j.jpain.2013.06.008](https://doi.org/10.1016/j.jpain.2013.06.008).
66. Chisholm KI, Khovanov N, Lopes DM, La Russa F, McMahon SB. Large scale *in vivo* recording of sensory neuron activity with GCaMP6. *eNeuro* 2018; 5: 0417–17. DOI: [10.1523/ENEURO.0417-17.2018](https://doi.org/10.1523/ENEURO.0417-17.2018).
67. Chen TW, Li N, Daie K, Svoboda K. A map of anticipatory activity in mouse motor cortex. *Neuron* 2017; 94: 866–879.e4. DOI: [10.1016/j.neuron.2017.05.005](https://doi.org/10.1016/j.neuron.2017.05.005).
68. Johannssen HC, Helmchen F. Two-photon imaging of spinal cord cellular networks. *Exp Neurol* 2013; 242: 18–26. DOI: [10.1016/j.expneurol.2012.07.014](https://doi.org/10.1016/j.expneurol.2012.07.014).
69. Christensen AJ, Iyer SM, Francois A, Vyas S, Ramakrishnan C, Vesuna S, Deisseroth K, Scherrer G, Delp SL. *In vivo* interrogation of spinal mechanosensory circuits. *Cell Rep* 2016; 17: 1699–1710. DOI: [10.1016/j.celrep.2016.10.010](https://doi.org/10.1016/j.celrep.2016.10.010).
70. Pnevmatikakis EA. Analysis pipelines for calcium imaging data. *Curr Opin Neurobiol* 2019; 55: 15–21. DOI: [10.1016/j.conb.2018.11.004](https://doi.org/10.1016/j.conb.2018.11.004).
71. Harding EK, Boivin B, Salter MW. Intracellular calcium responses encode action potential firing in spinal cord lamina I neurons. *J Neurosci* 2020; 40: 4439–4456. DOI: [10.1523/JNEUROSCI.0206-20.2020](https://doi.org/10.1523/JNEUROSCI.0206-20.2020).
72. Huang L, Ledochowitsch P, Knoblich U, Lecoq J, Murphy GJ, Reid C, de Vries SEJ, Koch C, Zeng H, Buice MA, Waters J, Li L. Relationship between simultaneously recorded spiking activity and fluorescence signal in GCaMP6 transgenic mice. *Elife* 2021; 10: e51675. DOI: [10.7554/eLife.51675](https://doi.org/10.7554/eLife.51675).
73. Wei Z, Lin BJ, Chen TW, Daie K, Svoboda K, Druckmann S. A comparison of neuronal population dynamics measured with calcium imaging and electrophysiology. *Plos Comput Biol* 2020; 16: e1008198. DOI: [10.1371/journal.pcbi.1008198](https://doi.org/10.1371/journal.pcbi.1008198).